IAA-AAS-DyCoSS1 -05-09

DESIGN OF TRANSFER TRAJECTORIES BETWEEN RESONANT ORBITS IN THE RESTRICTED PROBLEM WITH APPLICATION TO THE EARTH-MOON SYSTEM

Mar Vaquero* **and Kathleen C. Howell†**

The application of dynamical systems techniques to mission design has demonstrated that employing invariant manifolds and resonant flybys enables previously unknown trajectory options and potentially reduces the ΔV requirements. An analysis of two- and three-dimensional resonant orbits in the Earth-Moon system, as well as the computation and visualization of the associated invariant manifold structures is explored in this investigation. Three-dimensional maps are used to explore the relationship between the manifold trajectories associated with multiple resonant orbits and Earth departure trajectories. As a result, planar and three-dimensional homoclinic- and heteroclinic-type trajectories between unstable periodic resonant orbits are identified in the Earth-Moon system. To further illustrate the applicability of 2D and 3D resonant orbits in preliminary trajectory design, two planar transfers to the vicinity of L_5 and an out-of-plane transfer to a 3D periodic orbit that tours the entire Earth-Moon system are constructed exploiting the invariant manifolds associated with orbits in resonance with Moon.

INTRODUCTION

This investigation begins with the search, identification, and computation of three-dimensional resonant orbits bifurcating from planar resonant orbits in the circular restricted three-body problem (CR3BP), more specifically in the Earth-Moon system. The determination of the orbits and their application is facilitated by Poincaré sections, which are successfully employed to examine the relationship between the invariant manifolds associated with 3D unstable resonant orbits. The intersections of the invariant manifolds associated with these trajectories, as viewed in the Poincaré map, are then employed to search for potential resonance transitions. The resulting transfer trajectories benefit from a reduced maneuver cost (ΔV) by shadowing the invariant manifold trajectories. The core of this investigation is an exploration of resonance conditions in the Earth-Moon space by 1) cataloging 3D n-periodic orbits resonant with the Moon and 2) by searching for transfers between these orbits. As an application of resonant orbits in the Earth-Moon systems, a planar and a 3D transfer from Earth are presented.

The region of space in the Earth-Moon neighborhood has been previously investigated. Parker and Lo explore the use of unstable resonant orbits and their associated invariant manifolds to investigate mission scenarios near Earth involving periodic flybys of the Moon.[1] Anderson and Lo

*Ph.D. Student, School of Aeronautics and Astronautics, Purdue University, Armstrong Hall, 701 West Stadium Avenue, West Lafayette, Indiana 47907-2045.

†Hsu Lo Professor of Aeronautical and Astronautical Engineering, School of Aeronautics and Astronautics, Purdue University, Armstrong Hall, 701 West Stadium Avenue, West Lafayette, Indiana 47907-2045. Fellow AAS; Associate Fellow AIAA.

also complete a detailed analysis of the invariant manifolds emanating from resonant orbits involved in the Jupiter Europa orbiter (JEO) encounters, which are designed to exploit multiple gravity assists.[2,3,4,5] Vaquero and Howell extend the application of some of these techniques to the Saturn-Titan system,[6] introducing the design of a preliminary transfer to access the orbit of Hyperion, a moon of Saturn in resonance with Titan, by exploiting the invariant manifolds associated with periodic resonant orbits. The exploration of the Earth-Moon space, however, remains open and the goal of this investigation is to gain a better understanding of the dynamical structure in this regime. Some significant factors influence the behavior in the Earth-Moon region including the presence of only a single major natural satellite, i.e., the Moon. Additionally, the mass parameter, μ, is two and three orders of magnitude larger in the Earth-Moon system than in the Saturn-Titan and Jupiter-Europa systems, respectively; as a result, the effect of the Moon's gravity on the spacecraft is much larger, also affecting the stability of certain periodic orbits. Potentially, these very characteristics enable expanded trajectory design options and mission scenarios.

DYNAMICAL MODEL AND NUMERICAL METHODS

In any analysis involving resonance conditions, a resonance is typically defined initially within the context of the two-body problem and conics. However, this investigation is focused on resonance conditions involving multiple gravitational fields and, thus, the CR3BP serves as the basis for the problem formulation. In the restricted problem, the motion of an infinitesimal third particle, P_3, is modeled in the presence of two gravitationally-attracting bodies of significantly larger mass, P_1 and P_2. The motion of P_3 is governed by the well-known scalar, second-order differential equations of motion in standard form.[7] The state vector $\bar{X}$ is the six-element state vector $[x\ y\ z\ \dot{x}\ \dot{y}\ \dot{z}]^T$, where the dot indicates a derivative with respect to the non-dimensional time, τ, and relative to an observer in a rotating reference frame. The mass fraction μ is associated with the two system primaries P_1 and P_2, $\mu = \frac{m_2}{m_1+m_2}$, where m_1 and m_2 are the masses of P_1 and P_2, respectively. In this analysis, the value of the mass ratio used in the Earth-Moon system is $\mu \approx 0.0122$. The form of these equations of motion does admit an integral of the motion labeled the Jacobi constant, C, that is, $V^2 = 2U^* - C$, where the speed relative to the rotating frame is denoted V.

The existence of periodic motion in the CR3BP is well-known and its computation in the nonlinear system involves the use of a multi-dimensional version of a Newton-Raphson differential corrections process implemented as a shooting method. With the availability of the appropriate mathematical model, that is, the equations of motion and the state transition matrix (STM), the nonlinear differential equations are numerically integrated to any future time. The STM is essentially a linear map reflecting variational behavior in the vicinity of a trajectory arc and predicts adjustments in the initial state to shift the final state to a desired set of values at the end point. Thus, this approximation is used to adjust the initial state such that the current trajectory evolves and reaches some desired state downstream; with the appropriate constraints, a periodic orbit is generated. An infinite number of periodic orbits exist in the CR3BP. Lyapunov and halo orbits are examples of planar and out-of-plane periodic motion around the libration points. Resonant orbits, by definition, are periodic as well, but in contrast to Lyapunov or halo orbits, are not typically associated with a particular Lagrange point.

RESONANCE IN THE RESTRICTED THREE-BODY PROBLEM

Within the context of conics, a resonance exists when there is a simple numerical relationship between periods.[8] The focus of this investigation is orbit-orbit resonance, when the periods involved

represent the orbits of two or more bodies. Consider two bodies of arbitrary mass, denoted as A and B. In the two-body model, an orbit-orbit resonance is defined by the ratio p:q, where p indicates the period of motion for body B and q represents the period of motion for body A in resonance with body B. As an example, let the primary body represent Earth; thus, body A represents the Moon and body B models a spacecraft. The spacecraft is in orbital resonance with the Moon when it completes exactly p orbits about the Earth in the same time that is required for the Moon to complete q orbits. In this definition of orbital resonance, p and q are positive integers, and by convention, p is associated with the spacecraft and q reflects the period of the Moon. In the CR3BP, however, the p:q resonant ratio is not precisely equal to the ratio of the orbital periods corresponding to the bodies in resonance. In a multi-body problem, with the gravity of two or more bodies incorporated into the model, the time to complete a revolution is not even constant. Instead, for a p:q resonance in the circular restricted three-body problem, the spacecraft completes p orbits around the Earth in *approximately* the same time required for the Moon to complete q revolutions; thus, the ratio of the orbital periods is not rational, but rather an approximate rational fraction. However, actual resonant orbits in the CR3BP are still closed and periodic as observed in the rotating reference frame.

The addition of a third gravity field to the two-body model adds perturbations to the trajectory, generally resulting in a orbit that is not closed or periodic under perturbation. Hence, a strategy is required to compute closed, periodic, resonant orbits in the CR3BP and a simple targeting scheme is applied. A starting estimate for the initial state is generated from the two-body model. This starting vector seeds the corrections scheme to target a perpendicular crossing of the x-axis in a nonlinear propagation. Once a single, periodic, resonant orbit is determined, it is possible to generate multiple resonant orbits with the same characteristics, that is, a family of p:q resonant orbits, by employing a continuation scheme.

Planar and Three-Dimensional Resonant Orbits in the Earth-Moon System

Similar to families of libration point orbits, such as Lyapunov orbits, planar families of resonant orbits also include bifurcating orbits that intersect families of three-dimensional, periodic resonant orbits. These bifurcating orbits are identified by examining the eigenvalues of the monodromy matrix corresponding to each orbit in the family and the presence of a bifurcating orbit is indicated by an abrupt change in stability. Once the bifurcating orbit is identified, it is possible to target an out-of-plane orbit and, thus, 3D families. Once the bifurcating orbit is isolated, it is slightly perturbed in the z-direction and the resulting state seeds the corrections scheme to target a three-dimensional resonant orbit. Representative members from a selection of planar and 3D families of p:q resonant orbits in the Earth-Moon system are plotted in Figure 1. The 2D members appear in gray; the 3D orbits are plotted in blue. For completeness, Table 1 includes the non-zero initial conditions, the value of Jacobi constant and the orbital period corresponding to the smallest three-dimensional orbit represented in each family. The elements in the set of initial conditions with value zero are y, $\dot{x}$ and $\dot{z}$. Similar families of three-dimensional resonant orbits are straightforwardly computed for different values of the mass fraction μ.[6,7]

A particular class of resonant orbits in the Earth-Moon system has already proven to be useful in a mission scenario. The Interstellar Boundary Explorer (IBEX) is currently located in a long-term stable Earth orbit which is also in resonance with the Moon's orbit. The selection of this particular orbit for the extended IBEX mission was based on three major factors: minimization of the radiation dose, improvement of science collection and avoidance of long eclipses.[9] Based on this criteria, the spacecraft was recently maneuvered from its nominal trajectory into this new highly stable orbit in

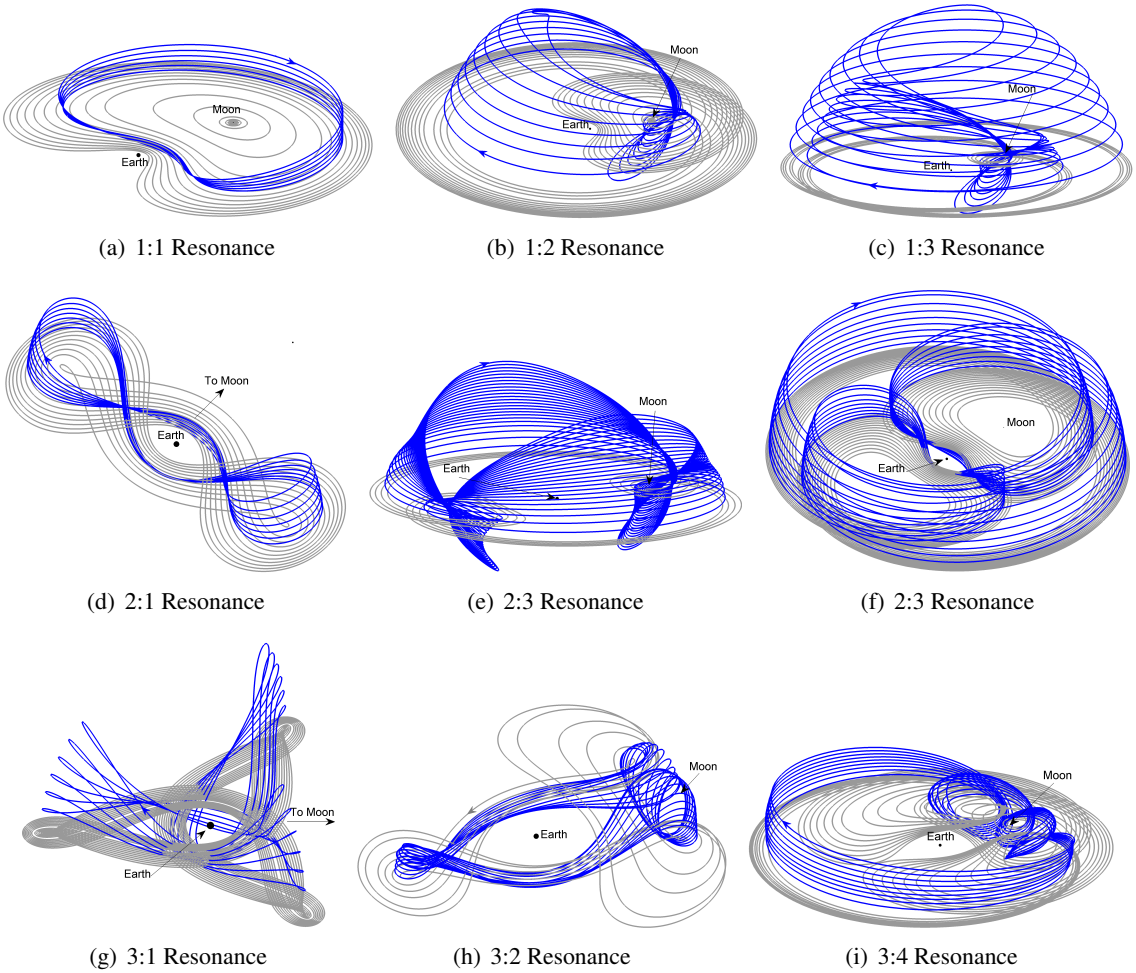

(a) 1:1 Resonance (b) 1:2 Resonance (c) 1:3 Resonance

(d) 2:1 Resonance (e) 2:3 Resonance (f) 2:3 Resonance

(g) 3:1 Resonance (h) 3:2 Resonance (i) 3:4 Resonance

Figure 1. Representative Orbits in Planar and Three-Dimensional Families of *p*:*q* Resonant Orbits in the Earth-Moon System - Plotted in the Rotating Frame

Table 1. Non-Zero Initial Conditions and Jacobi Constant Value Corresponding to the First (Smallest in z) Three-Dimensional Resonant Orbit in each *p*:*q* family

p:*q*	x (km)	z (km)	$\dot{y}$ (km/sec)	C	P (days)
1:1	1.0339×10^5	-384.4	2.2364	2.3696	27.1033
1:2	3.3005×10^5	-3,844.0	0.6491	2.7921	48.7944
1:3	3.1902×10^5	-3,844.0	0.7067	2.7126	78.0086
2:1	7.1994×10^4	-3844.0	2.7495	2.7575	27.2489
2:3	3.4058×10^5	-384.4	0.6241	2.8523	73.5564
2:3	8.4946×10^4	-384.4	2.6140	2.0454	81.5908
3:1	-3.0025×10^5	19,220.0	0.0544	3.1850	27.1874
3:2	2.6870×10^5	-384.4	0.6232	2.9808	52.0254
3:4	3.5408×10^5	-384.4	0.6362	2.9440	94.9389

a 3:1 resonance with the Moon. IBEX's extended orbit resembles one of the 3D orbits plotted in Figure 1(g). This type of resonant orbit, along with other lunar resonant orbits, might be useful for many types of missions, including weather and space science applications.[10]

Poincaré Maps and Invariant Manifolds

In general, maps are used to describe the time evolution of a vector at discrete intervals. The use of very simple maps allows the representation of the properties of generic dynamical systems that are described by the differential equations. Maps have been used extensively in the last few decades, especially to add insight and expose dynamical structure within complex systems. This technique offers three main advantages: reduction of dimension, global dynamics, and conceptual clarity.

For the planar CR3BP in $\Re^4$, the surface of section, or hyperplane Σ, is typically specified by fixing one of the coordinates, usually $y = 0$, producing a surface in $\Re^3$. The 3D surface is projected onto a plane by specification of another parameter. For example, to generate a two-dimensional Poincaré section in the CR3BP, a value for the Jacobi constant is specified and a grid of initial conditions for x and $\dot{x}$ are selected and integrated forward in time. The intersections of each trajectory with the surface of section create the Poincaré map. With C, x and $\dot{x}$ initially defined, as well as the hyperplane $y = 0$, the corresponding initial values for $\dot{y}$ can be calculated from the expression for the Jacobi constant, that is,

$$\dot{y} = \pm\sqrt{x^2 + y^2 + \frac{2(1-\mu)}{d} + \frac{2\mu}{r} - \dot{x}^2 - C} \tag{1}$$

where d and r are evaluated as $d = \sqrt{(x+\mu)^2 + y^2 + z^2}$ and $r = \sqrt{(x-1+\mu)^2 + y^2 + z^2}$. The quantities used to plot the intersections in this investigation are usually x and $\dot{x}$, although other quantities are also considered, such as Delaunay variables, as well as other dynamical quantities.[2]

In this investigation, the analysis and construction of three-dimensional transfer trajectories is completed with the aid of higher-dimensional maps. However, the spatial problem in $\Re^6$ presents some challenges. The surface of section, Σ, is specified in a similar way, that is, by fixing one of the coordinates, usually $y = 0$, and producing a surface in $\Re^5$. The dimension of the problem is further reduced by the specification of another parameter, such as Jacobi constant, C. In this analysis, to represent a trajectory on a higher-dimensional map (4D), three coordinates are used, i.e., x and $\dot{x}$ in the plane and z along the vertical axis, and a non-physical quantity reflects the value of the third component of the velocity, i.e., $\dot{z}$. Then, the corresponding value for $\dot{y}$ is calculated from the expression for the Jacobi constant in Eq. (1). One option to represent the fourth dimension or component in a 3D figure is the use of an arrow of varying length. At the manifold crossing $(x, \dot{x}, z)$ in the 3D figure, a second coordinate system representing velocity space is introduced ($\dot{x}, \dot{y}, \dot{z}$ labeled V_x, V_y, V_z). Directional arrows are added in an attempt to qualitatively represent the direction of the velocity associated with the manifold at the crossing and are scaled according to the magnitude of the $\dot{z}$ component.

The role of invariant manifolds is significant in building a framework to model the dynamical structure in the CR3BP. Knowledge of any manifold structure improves the efficiency of trajectory design in this regime. The use of invariant manifolds in the design of transfers between resonant orbits in the Earth-Moon system is the focus of this effort. Once the periodic orbits and their associated invariant manifolds are identified, the search for potential transfers to and from these orbits requires the computation of the actual unstable and stable manifolds. The invariant manifolds corresponding to a periodic orbit essentially represent the flow to and from the orbit and are frequently

computed by using the eigenvector corresponding to the unstable and stable eigenvalues, denoted λ_u and λ_s, respectively.[6] An offset value of 30 km is used in the computation of the stable and unstable manifolds associated with periodic orbits in the Earth-Moon system.

RESONANCE TRANSITION

The trajectories along the invariant manifolds corresponding to unstable resonant orbits possess their own distinctive behavior. However, the arcs are tangled, so plotting these paths in the *xy*-plane does not offer any clear insight. In contrast to libration point orbits, the trajectories along the resonant orbit manifolds frequently pass close to different resonances, but also remain in the vicinity of the original resonant orbit in configuration space.[2] A Poincaré section that reflects the behavior in the vicinity of these resonant periodic orbits as well as the manifolds also emerges. Maps that identify, and potentially isolate, these manifold trajectories aid in visualization and offer clues concerning the relationships between these manifolds and other structures in the phase space. Once potential resonance transitions are identified from the maps, a corrections scheme is employed to blend the periodic orbits and the manifolds arcs into a continuous path.

Natural Transfers between Two-Dimensional Resonant Orbits

The relationship between planar stable and unstable orbits resonant with Titan and Europa has been previously explored.[2,6,7] Anderson and Lo examine various techniques in considering low-energy trajectory design for missions to Europa, as well as the Europa Orbiter (EO) spacecraft. In their investigations, Lo and Anderson first use Poincaré sections to search for unstable resonant orbits in support of the Europa Orbiter mission concept.[3,4,5] The invariant manifolds from these unstable resonant orbits reflect the transitions of the actual EO trajectory between resonances. The actual trajectory clearly exploits invariant manifolds associated with quasi-periodic orbits.[4] Anderson also presents a flyby design that exploits heteroclinic and homoclinic connections of resonant orbits in the Jupiter-Europa system.[11] Extending the work of Lo and Anderson, Vaquero and Howell apply some of these techniques to the Saturn-Titan system with emphasis on three-dimensional resonant orbits. More specifically, their investigation focuses on the analysis and design of planar trajectories that transition between interior and exterior resonant orbits as well as between libration point orbits in the Saturn-Titan system.[6] Similar relationships between planar resonant orbits exist in the Earth-Moon system.

In this analysis of the natural dynamics associated with resonant orbits in the Earth-Moon regime, natural connections between 2D resonant orbits are examined. As an illustrative example of the existence of 'natural' transfer trajectories between these type of orbits, consider the planar 1:2 and 2:3 periodic resonant orbits plotted in Figures 2(a)-2(b). For completeness, the non-zero initial state, orbital period, Jacobi constant value and unstable eigenvalue associated with these two periodic orbits are listed in Table 2. The invariant manifolds associated with these periodic orbits, in resonance with the Moon, are computed using an offset value of 30 km and a total of 10,000 fixed points evenly spaced in time along the orbits. The trajectories along the stable manifold tube are propagated backwards in time for 40 non-dimensional time units, equivalent to 174 days. Similarly, the trajectories along the unstable manifold tube are integrated forward in time for the same interval. For a wider view of the invariant manifolds and their relationship to other dynamical structures, it is necessary to plot them against a background that includes some of these structures. The set of initial conditions used to generate this surface of section is selected to be in the vicinity of the periapsis of the resonant orbits of interest. An integration time of approximately 7 years is employed to generate

the one-sided background maps in Figs. 2(c)-2(d). The quantities used in plotting are position and velocity, that is, x and $\dot{x}$, labeled V_x on the map.

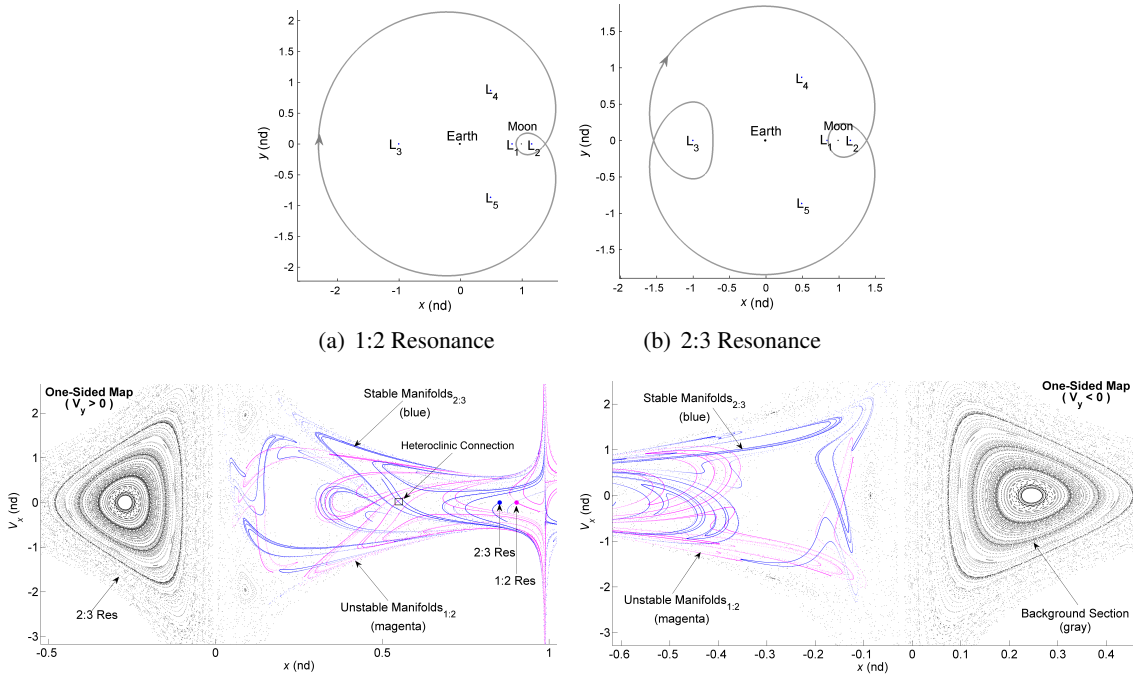

(a) 1:2 Resonance (b) 2:3 Resonance

(c) One-Sided Poincaré Map ($\dot{y} > 0$) (d) One-Sided Poincaré Map ($\dot{y} < 0$)

Figure 2. Two-Dimensional (a) 1:2 and (b) 2:3 Resonant Orbits in the Earth-Moon System (Moon x2) and (c)-(d) 2D Surface of Section Illustrating the Stable (Blue) and Unstable (Magenta) Manifolds Associated with the 2:3 and 1:2 Resonant Orbits

Table 2. Non-Zero Initial Conditions, Jacobi Constant Value, Orbital Period and Unstable Eigenvalue Corresponding to the 1:2 and 2:3 *Two*-Dimensional Resonant Orbits in Figure 2(a) and Figure 2(b)

p:q (2D)	x (km)	$\dot{y}$ (km/sec)	C	P (days)	λ_u
1:2	3.4697×10^5	0.6728	2.8284	47.6002	-59.8418
2:3	3.2759×10^5	0.6170	2.8284	74.6037	-85.2575

An intersection in the Poincaré map is an intersection in phase space. That is, an intersection of the stable and unstable manifolds associated with a periodic orbit on the Poincaré section – generated for a particular value of Jacobi constant – is a point that approaches the orbit when integrated into the future as well as into the past.[2] Such a trajectory is frequently termed a 'homoclinic' connection. Similarly, an intersection of the stable and unstable manifolds associated with two different periodic orbits on the Poincaré section is a point that approaches one of the periodic orbits when integrated into the future and the other periodic orbit when integrated into the past. Such a trajectory is known as a 'heteroclinic' connection. As illustrated on the one-sided surfaces of section plotted in Figures 2(c)-2(d), multiple homoclinic and heteroclinic trajectories exist between the 1:2 and 2:3 resonant orbits at $C = 2.8284$. For illustration purposes, three connections are detailed in this analysis; a heteroclinic connection and two homoclinic trajectories between each resonant orbit of interest. The heteroclinic connection is computed from an intersection of the unstable manifolds as-

sociated with the 1:2 resonant orbit and the stable manifolds associated with the 2:3 resonant orbit. The actual intersection in phase space is labeled on the map in Figure 2(c); the unstable manifolds appear in magenta and the stable manifolds are plotted in blue. At the intersection, the unstable manifold crossing is propagated in reverse time until it reaches the 1:2 resonant orbit; the stable manifold crossing is propagated in forward time until it reaches the 2:3 resonant orbit. The two resulting manifold arcs are decomposed into smaller subarcs that seed a multiple shooting algorithm. In the corrections scheme, continuity in position and velocity at each intermediate patch point is enforced, producing a natural, maneuver-free path that departs the 1:2 resonant orbit and approaches the 2:3 resonance. The resulting heteroclinic trajectory appears plotted in Figure 3(a). Recall that a homoclinic connection is calculated from the intersection of the stable and unstable manifolds associated with the same periodic orbit. The homoclinic connection in Figure 3(b) asymptotically departs and approaches the 1:2 resonance in forward and backward time; similarly, the homoclinic connection in Figure 3(c) asymptotically departs and approaches the 2:3 resonance in forward and backward time. To aid in the visualization of the trajectory, the 1:2 and 2:3 resonant orbits appear plotted in magenta and blue, respectively.

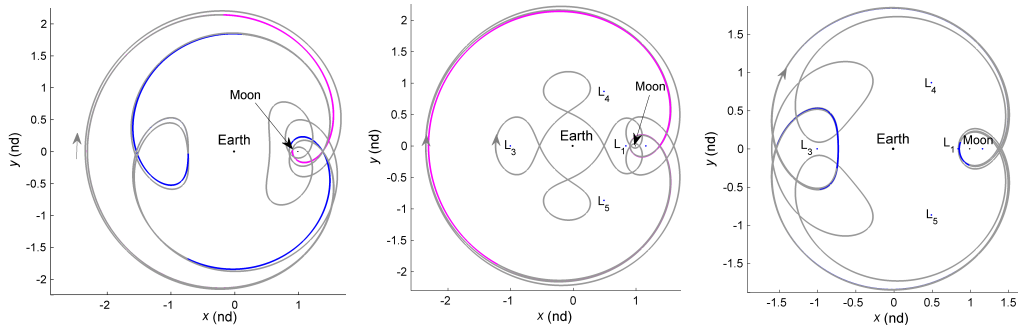

(a) Heteroclinic Connection (b) Homoclinic Connection (1:2) (c) Homoclinic Connection (2:3)

Figure 3. Two-Dimensional Heteroclinic and Homoclinic Connections Between 1:2 and 2:3 Resonant Orbits Plotted in the Rotating Frame (Moon x2)

In some cases, it may be possible to numerically correct these type of natural trajectories to obtain periodic orbits that shadow the invariant manifolds associated with one or more resonant orbits of interest, thus, creating a cycle between resonances. Consistent with previous resonant orbits, a family of periodic resonant cycles can be generated, although the existence of such a family is dependent on the relationship between their associated invariant manifolds. That is, the existence of a family of resonant cycles is limited to the existence of a connection between the associated invariant manifolds.[6]

Natural Transfers between Three-Dimensional Resonant Orbits

The relationship between unstable resonant orbits in the Earth-Moon system is not unique to the planar case. Similar three-dimensional trajectories between resonant orbits that follow the natural dynamics of the system also exist. To illustrate some of the three-dimensional results, consider the unstable, 3D, 'southern' 1:2 resonant orbit at $C = 2.5945$ as illustrated in Figure 4. This orbit, resonant with the Moon, is symmetric across the xz-plane, assuming that the initial state is located such that $y_0 = 0$, then $\dot{x}_0 = \dot{z}_0 = 0$. For visualization purposes, the projections of the 3D orbit onto the xy-plane and xz-plane appear in Figures 4(b)-4(c), respectively. The non-zero initial

conditions, period and unstable eigenvalue for the 3D periodic orbit are listed in Table 3. Once an unstable resonant orbit is identified, the associated invariant manifolds are computed and displayed in a surface of section. The invariant manifolds computed in conjunction with the 1:2 resonant orbit in Figure 4 are displayed in Figure 5 and appear as a 3D-projection of a 4D surface of section. The stable and unstable manifolds are plotted in blue and magenta, respectively. Two-dimensional views are represented in Figures 5(b)-5(c). The fixed points associated with the periodic orbit are displayed on the map as black dots. Note that although not visible in Figure 5, directional arrows reflect the direction of the velocity and the magnitude of $\dot{z}$ at each crossing and thus, represent the 4th dimension.

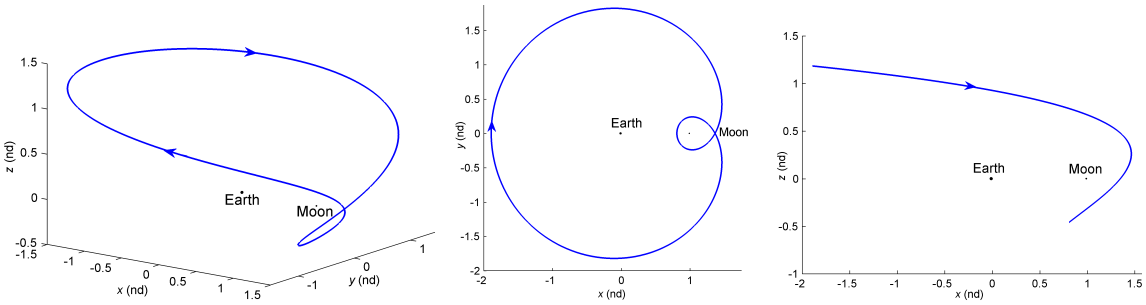

(a) xyz-view (b) xy-view (c) xz-view

Figure 4. Three-Dimensional 'Southern' 1:2 Resonant Orbit in the Earth-Moon System (Moon x2)

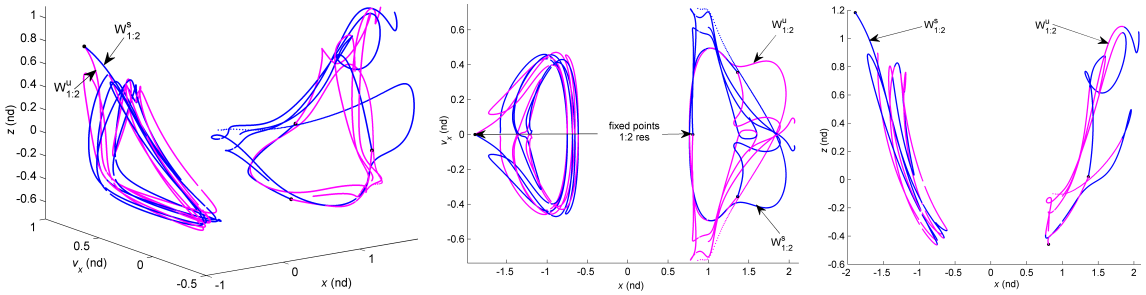

(a) xyz-view (b) xy-view (c) xz-view

Figure 5. Position-Velocity Representation of the Stable (Blue) and Unstable (Magenta) Manifolds Associated with the 1:2 Resonant Orbit in Fig 4.

The focus of this analysis is the computation of the transitions between resonant orbits employing manifold arcs, so the next step is the identification of other resonant orbits in the vicinity of the intersections of the unstable and stable manifolds on the 4D map. Points on the map with $\dot{x} = \dot{z} = 0$ and near the intersection of the manifolds are sought as 3D resonant candidates. Using two-body approximations and a corrections algorithm, a new resonant orbit is generated. As an illustrative example, a 2:3 'southern' resonant trajectory is computed and represented in Figure 6. This new periodic orbit possesses the same value of Jacobi constant as the 1:2 resonant orbit in Figure 4, that is, $C = 2.5945$. For completeness, the non-zero initial conditions and period associated with this orbit are listed in Table 3.

As illustrated in Figure 5, the invariant manifolds associated with 3D resonant orbits form well-defined, almost closed contours when represented in terms of position and velocity components, that

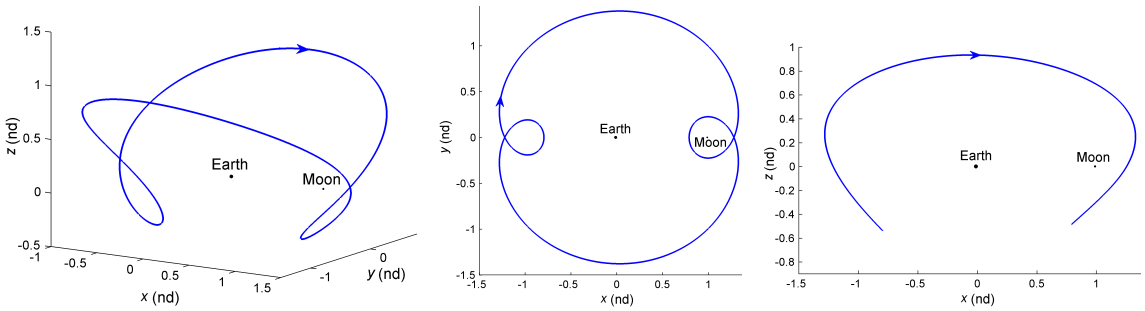

(a) xyz-view (b) xy-view (c) xz-view

Figure 6. Three-Dimensional 2:3 'Southern' Resonant Orbit in the Earth-Moon System (Moon x2)

Table 3. Non-Zero Initial Conditions, Jacobi Constant Value, Orbital Period and Unstable Eigenvalue Corresponding to the 1:2 and 2:3 *Three*-Dimensional 'Southern' Resonant Orbits in Figures 4 and 6

p:q (3D)	x (km)	z (km)	$\dot{y}$ (km/sec)	C	P (days)	λ_u
1:2	-7.2754$\times 10^5$	4.5493$\times 10^5$	1.4065	2.5945	53.8195	38.5570
2:3	3.0382$\times 10^5$	-1.8687$\times 10^5$	0.4373	2.5945	80.9323	163.1938

is, x, $\dot{x}$ and z. From the representation of the invariant manifolds Figure 5, it is possible to locate intersections between the stable and unstable manifolds associated with one or more resonant orbits of interest to yield 'natural' connecting paths. Such an intersection in phase space is determined from an intersection on the 4D map where the values of x, $\dot{x}$ and z are the same and the corresponding directional arrows are parallel in orientation (direction) and possess the same length. Since all the manifold trajectories are computed at the same energy level, the corresponding value for $\dot{y}$ can be recovered from the expression for Jacobi constant. Lastly, the surface of section is defined at $y = 0$, so both trajectories share this value at the intersection. Because only a finite number of stable and unstable manifolds trajectories are computed, it may not be possible to locate an 'exact' intersection on the 4D map. However, nearby intersections are clearly identifiable from Figure 5 and with the aid of a corrections algorithm it is possible to remove the small difference that may exist in the position and velocity states. Thus, once a potential connection is identified, the point at the intersection on the map associated with the stable manifold is propagated forward in time and the point at the intersection associated with the unstable manifold is propagated backward in time until each manifold trajectory reaches the associated resonant orbit. Then, each manifold arc is decomposed into smaller subarcs to reduce the sensitivities in the numerical corrections process. A multiple shooting algorithm is employed to reconnect the subarcs and remove the small discontinuity that exists, yielding a three-dimensional trajectory continuous in position and velocity.

In the planar problem, an intersection in the Poincaré map is an intersection in phase space. That is, a homoclinic connection can be generated from an intersection on the map of the stable and unstable manifolds associated with a given periodic orbit. Similarly, a heteroclinic connection can emerge from an intersection of the stable and unstable manifolds associated with two different periodic orbits. In the spatial problem, similar connecting paths are computed with the aid of a 4D map and a robust corrections scheme. In this analysis, the 3D path, continuous in position and velocity, is termed a 'homoclinic-type' trajectory if the connected manifolds are associated with one resonant orbit; it is labeled a 'heteroclinic-type' trajectory if the connected manifolds

are associated with two resonant orbits. Recall that a multiple shooting algorithm is employed to numerically correct these type of trajectories. In such scheme, continuity in position and velocity are enforced at each patch point, but other constraints are also specified to ensure that the resulting trajectory departs and approaches the resonant orbit(s) of interest. That is, each manifold trajectory is propagated forward (stable) or backward (unstable) in time until the trajectories wrap around the resonant orbit(s) for two revolutions. After propagation, the position of the end points on each manifold arc is fixed and the value of Jacobi constant is enforced to guarantee that the resulting transfer is at the same energy level as the two periodic orbits of interest.

As an illustrative example of such three-dimensional connections between resonant orbits in the Earth-Moon system, consider the unstable resonant orbits represented in Figures 4 and 6. The invariant manifolds associated with these resonant trajectories are employed as transfer mechanisms between the orbits. A homoclinic-type connection asymptotically departs and approaches the same resonant orbit when propagated forward and backward in time. As an illustrative example, consider a 3D homoclinic-type trajectory associated with the 1:2 resonance in Figure 4. A 4D map representing the stable (blue) and unstable (magenta) manifolds associated with this 1:2 resonant orbit appears in Figures 7(a)-7(b). For visual clarity, only the directional arrows at the intersection are represented in Figure 7(b). The magenta and blue arrows are associated with the unstable and stable manifolds, respectively. Recall that the direction of these arrows indicates the velocity direction at each crossing; the arrows are scaled according the magnitude of the out-of-plane component of the velocity, i.e. $\dot{z}$, at the crossing of the hypersurface. A similar approach is employed to remove the discontinuity that exists in both position and velocity; the resulting out-of-plane trajectory is plotted in Figure 7(c). For visualization purposes, two-dimensional views of the 3D trajectory on the xy- and xz-plane are represented in Figures 7(d)-7(e).

Another type of natural connecting path that exploits the invariant manifolds associated with two different resonant orbits can also be computed at this particular value of Jacobi constant. That is, a heteroclinic-type connection is available from the intersection of the stable manifolds associated with one of the orbits and the unstable manifolds associated with the other resonant orbit; in this particular example, a 1:2 and a 2:3 resonant orbit. A heteroclinic-type trajectory exists from each orbit, that is, asymptotically departing the 1:2 resonance and approaching the 2:3 resonant and vice versa. As an illustrative example, consider a 3D heteroclinic-type connection asymptotically departing the 1:2 resonance and asymptotically approaching the 2:3 resonant orbit. A 4D map representing the unstable manifolds associated with the 1:2 resonant orbit (magenta) and the stable manifolds associated with the 2:3 resonant orbit (blue) is generated and represented in Figure 8(a). The invariant manifolds are propagated for 217 days. The map intersection that is employed to generate the stable and unstable manifold arcs is also highlighted in Figure 8(a). Recall that, at this intersection, the trajectories share very similar values of x, $\dot{x}$ and z and the associated directional arrows at the crossing are oriented along the same direction and possess approximately the same length, which indicate a match in the $\dot{z}$ component as well. The resulting three-dimensional 'natural' trajectory that transitions between the two resonances in the Earth-Moon system appears in Figure 8(b). Note that this trajectory is continuous in position and velocity. The corrections process is already incorporated to remove the small discontinuity that exists between the states obtained from the intersection highlighted on the map in Figure 8(a).

The natural connecting paths in Figure 7 and Figure 8 are not unique to these particular resonances. In fact, similar trajectories are computed for other resonant orbits at this particular energy level. Note that the two 3D resonant orbits in Figures 7-8 are denoted 'southern' resonant orbits.

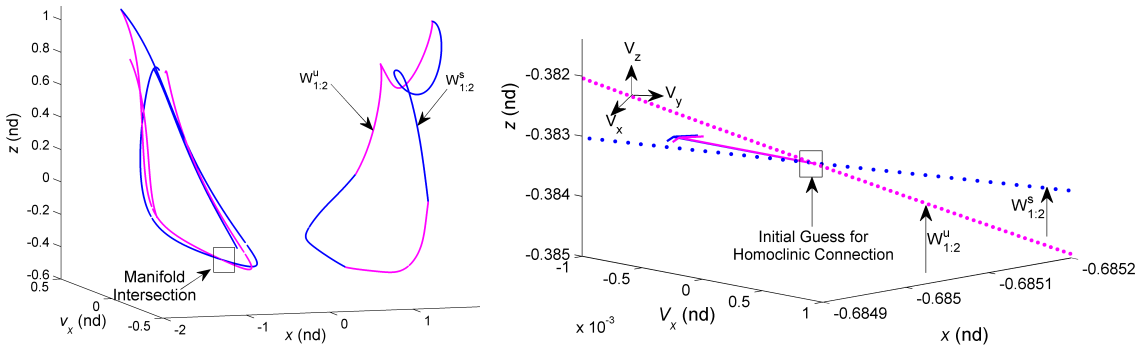

(a) Manifold Representation (b) Zoomed View of Initial Guess

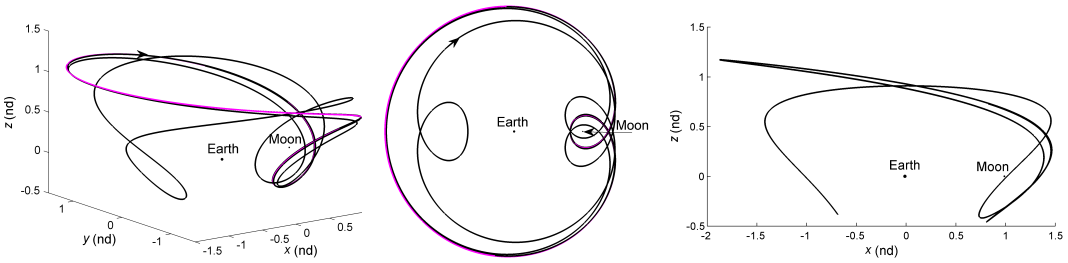

(c) xyz-view Homoclinic (d) xy-view Homoclinic (e) xz-view Homoclinic

Figure 7. (a)-(b) Higher-Dimensional Surface of Section Illustrating Stable (Blue) and Unstable (Magenta) Invariant Manifolds and (c)-(e) Three-Dimensional Homoclinic-Type Transfer Trajectory Between a 1:2 Resonant Orbit in the Earth-Moon System

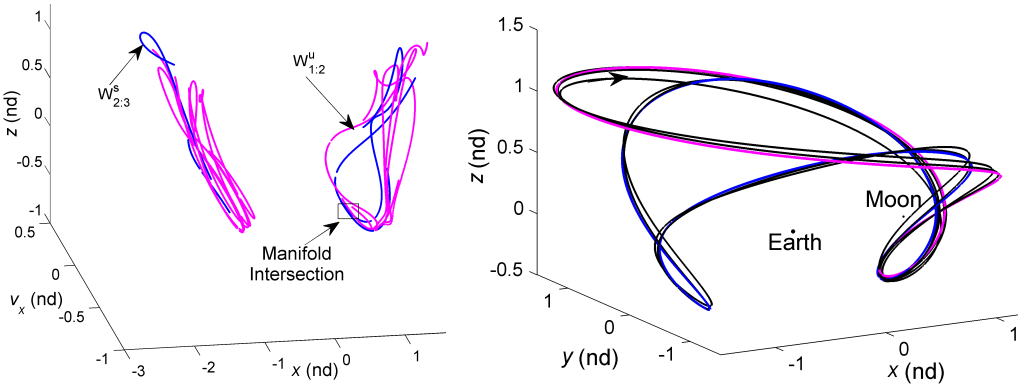

(a) Manifold Representation (b) 3D Heteroclinic-Type Connection

Figure 8. Higher-Dimensional Surface of Section Illustrating Stable (Blue) and Unstable (Magenta) Invariant Manifolds and Three-Dimensional Heteroclinic-Type Transfer Trajectory Between a 1:2 and a 2:3 Resonant Orbit

The 'northern' counterparts also exist and are computed with the same numerical scheme. Similar natural transfer trajectories also exist between the northern periodic orbits.

APPLICATIONS OF MANIFOLD TRANSFER TRAJECTORIES

A recent strategy in trajectory design involves the exploitation of the invariant manifolds associated with resonant orbits. In this investigation, this concept is employed to generate orbits in the

Earth-Moon system. A design process is described that yields continuous trajectories that depart from and arrive at selected periodic orbits. For demonstration, manifold arcs associated with unstable periodic orbits are used exclusively and Poincaré maps aid in the visualization of these invariant manifold trajectories in phase space. A multiple-shooting algorithm then blends the subarcs into a single continuous trajectory, enforcing continuity in position and allowing maneuvers at intermediate locations to accommodate any discontinuities that may exist in velocity. Two illustrative examples follow: (i) a planar transfer from Earth to the vicinity of the equilateral point L_5 via an unstable manifold arc associated with a planar 4:3 resonant orbit, and (ii) an out-of-plane transfer from Earth to a 3D periodic orbit that tours the entire system, that is, the orbit of the Moon (above and below the orbital plane) and the collinear libration points L_1, L_2 and L_3.

Planar Transfer Trajectories from Earth to the Vicinity of L_5

The effect of the Moon on periodic resonant orbits around the Earth can be significant, potentially delivering useful transfer scenarios. The large value of the mass parameter, μ, also influences the stability of the orbits in resonance with the Moon. Periodic resonant orbits in a family defined in terms of a p:q resonant ratio may be unstable in the Earth-Moon system but linearly stable in other systems. For example, consider the family of 4:3 resonant orbits in the Earth-Moon system plotted in Figure 9(a). Representative members in the same family of 4:3 resonant orbits in the Saturn-Titan system appear in Figure 9(b). The effect of the Moon, through a higher mass ratio, on the periodic orbits compared to the effect of Titan on orbits with very similar characteristics is immediately obvious. If stability is assessed using the monodromy matrix, then an eigenvalue $|\lambda|$ with magnitude greater than one indicates an unstable periodic orbit. Using this criteria, all members in the 4:3 resonant family in the Earth-Moon system are unstable, with the largest unstable eigenvalue $|\lambda_u| = 2,513.2$. In contrast, most of the 4:3 resonant orbits in the Saturn-Titan family are linearly stable; only a few orbits possess an unstable eigenvalue of magnitude $|\lambda_u| = 1.4704$. The Moon also affects the period of these resonant orbits. Recall that the addition of a third gravity field to the system adds perturbations on the trajectories. As a consequence, the resonant ratio is not exactly equal to the value in the two-body model, but, rather, is an approximate rational fraction. A larger value of the mass parameter influences the value of the resonant period to a greater degree. The large perturbation also adds a challenge in the computation of periodic resonant orbits. The initial conditions that produce a resonant orbit in the two-body model are generally not sufficiently accurate to produce a good initial guess for a resonant orbit in the Earth-Moon system, so a modification of the initial conditions is required to target the desired periodic orbit.

The planar periodic orbits in resonance with the Moon that are illustrated in Figure 9(a) offer a continuous "tour" of the system, that is, a spacecraft placed in one of these orbits travels to the general vicinities of the five libration points as well as the Moon. Therefore, these orbits are candidates for transfers to the vicinity of the libration points. As an application of the use of planar resonant orbits in the design of transfer trajectories in the Earth-Moon system, consider a transfer to the vicinity of the equilateral point L_5. The periodic orbit plotted in Figure 9(c) is selected from the 4:3 family in Figure 9(a) to serve as a basis for a transfer but other members in the family can also be employed. An initial Earth orbit and a final periodic orbit at L_5 are incorporated, as well as two different intermediate arcs, to construct the transfer from Earth to the vicinity of L_5. Thus, the following arcs are blended into a path continuous in position: (i) An initial Low Earth Orbit (LEO) with an altitude of 180 km, (ii) an Earth departure leg, (iii) a stable manifold arc associated with the 4:3 resonant orbit, and, (iv) an arrival short period orbit around L_5. A total of three maneuvers are incorporated along the transfer path. A tangential maneuver initiates the departure from the 180 km

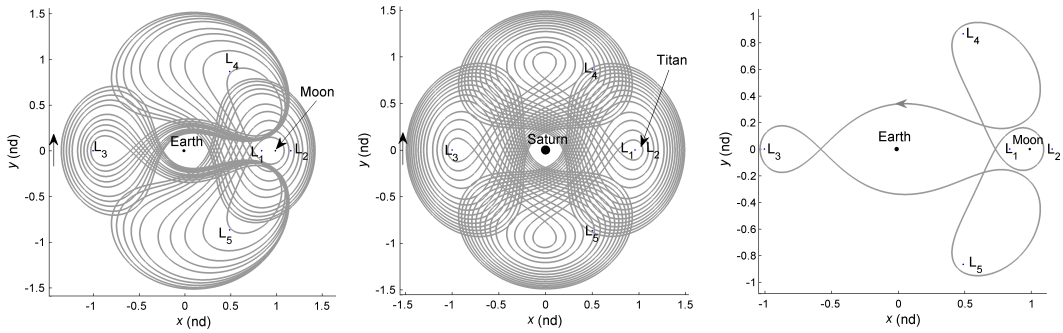

(a) Earth-Moon System (b) Saturn-Titan System (c) Selected 4:3 Resonant Orbit

Figure 9. Representative Members in a Family of 4:3 Resonant Orbits in the Earth-Moon ($\mu \approx 0.0122$) and Saturn-Titan ($\mu \approx 2.3658 \times 10^{-4}$) Systems in (a) and (b). Selected Periodic Orbit in the Earth-Moon System for a Transfer Trajectory to L_5 in (c) - Plotted in the Rotating Frame

altitude LEO orbit where the spacecraft is initially located. A second maneuver connects the Earth departure leg to the stable manifold arc. Skipping the second maneuver, allows the spacecraft to asymptotically approach the 4:3 resonant orbit. Finally, a third maneuver along the stable manifold arc yields an insertion into the selected arrival orbit around L_5.

Once the initial and final orbits are selected, it is necessary to identify appropriate intermediate arcs to connect the orbits of interest. Thus, the next step in this transfer design process is the computation of the stable manifold trajectories associated with the 4:3 unstable orbit. This sample transfer is planar and, thus, the stable manifolds are displayed on a one-sided surface of section located at $y = 0$. The resulting Poincaré map aids in (i) visualizing the stable manifolds in phase space, and (ii) in locating regions of potential intersections that may yield low-cost connections between the two intermediate arcs, that is, the Earth departure leg and the stable manifold arc. For potential connections between these two arcs, multiple Earth departure options are also computed and displayed on the same surface of section. The various Earth departure legs are constructed by adding maneuvers at different locations along the low Earth orbit. The magnitude of the first maneuver (ΔV_1) is such that the value of Jacobi constant corresponding to the resulting Earth departure leg equals the energy value corresponding to the stable manifold arc, i.e., the energy value of the resonant orbit. To compute a range of possible Earth departure trajectories, an angle θ is defined to parametrize the position of the spacecraft along the circular orbit, such that $0 \leq \theta \leq 2\pi$. A tangential maneuver such that $C_{Earth_{Leg}} = C_{Manifold}$ is then applied at each location and the resulting states are propagated forward in time to a crossing of the hyperplane. Recall that the selected resonant orbit for this application is plotted in Figure 9(c); it possesses a Jacobi constant value of $C = 2.9006$ and an unstable eigenvalue of $|\lambda_u| = 2,546.6$. The resulting one-sided Poincaré maps appear in Figures 10(a)-(b). The stable manifold crossings are plotted in blue and the crossings of the various Earth departure legs appear in magenta. These trajectories are plotted against a background map (gray) that highlights other dynamical structures at this particular energy level in the vicinity of the Earth and the Moon. Recall that the quantities used in plotting the crossings with the hyperplane are in nondimensional units. For reference, the Earth is located at $x = -\mu = -0.0122$ and the Moon is located at $x = 1 - \mu = 0.9878$. The set of initial conditions used to generate this background surface of section is selected to be in the vicinity of the resonant orbit of interest. A planar problem, the bounds are defined with $y = 0$ and $z_0 = \dot{z}_0 = 0$; recall that the corresponding value of $\dot{y}_0$

is calculated from the value of Jacobi constant. In propagating the initial conditions, longer integration times are necessary to produce sufficient crossings to yield a dense and well-defined map. For this particular example, an integration time of approximately 1.8 years is employed to generate the background map in Figure 10. The nondimensional quantities used in plotting are position and velocity, that is, x and $\dot{x}$, labeled V_x on the map.

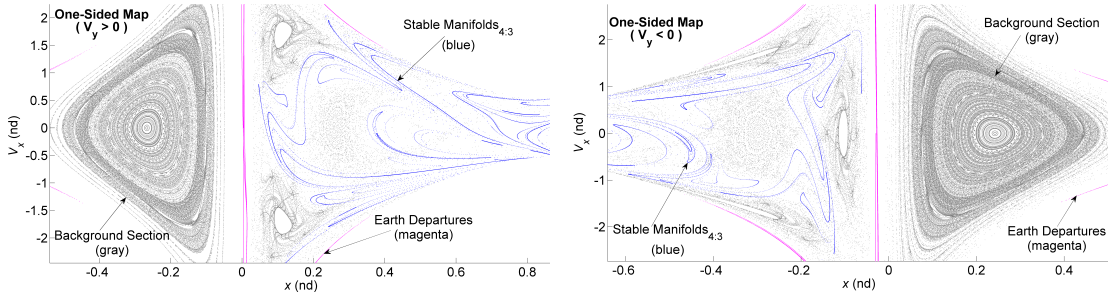

(a) One-Sided Map ($\dot{y} > 0$)

(b) One-Sided Map ($\dot{y} < 0$)

Figure 10. Poincaré Maps Illustrating the Relationship between the Stable Manifolds (Blue) and the Selected Earth Departure Legs (Magenta)

A natural, cost-free, transfer path between an Earth departure trajectory and a stable manifold arc can be computed from an intersection between the magenta (Earth departures) and blue (stable manifolds) crossings on the map. If such an intersection exists on the map, no $\Delta\bar{V}$ is required to connect the intermediate arcs. However, no such intersections appear in Figure 10. In fact, all the Earth departure crossings are located along the boundary region on the map whereas the stable manifold crossings possess smaller $\dot{x}$ components. However, it is possible to locate nearby intersections that may yield reasonable connections that reach the insertion point along a short period L_5 orbit. Once all the segments have been selected, a multiple-shooting corrections scheme is used to enforce continuity in position and velocity except at departure, arrival, and at the intermediate locations, where maneuvers ($\Delta\bar{V}_s$) are allowed. Several different scenarios are available using this technique, but only two are summarized here. The two transfer trajectories that employ a stable manifold arc associated with the 4:3 resonant orbit to reach the vicinity of L_5 are illustrated in Figure 11 and Figure 12. The Earth departure arc is represented in magenta, the stable manifold arc appears in blue and the selected arrival short period orbit around L_5 is plotted in black. The total cost (ΔV_T) and time of flight (TOF) associated with these transfer trajectories from Earth to L_5 are detailed in Table 4. Note that these transfers are not optimized.

Table 4. Maneuver Cost and Time of Flight Associated with Transfer Trajectories A and B

Transfer	ΔV_1 (km/s)	ΔV_2 (m/s)	ΔV_3 (km/s)	ΔV_T (km/s)
A	3.1132	400.6702	195.3726	3.7092
B	3.1141	272.1777	288.2255	3.6745
	TOF_E (days)	TOF_M (days)	TOF (days)	P_{L_5} (days)
A	2.2014	43.8926	46.0939	28.5504
B	4.3072	23.3814	27.6886	28.5504

Transfer trajectory A is computed by employing arcs at the same energy level from the maps in

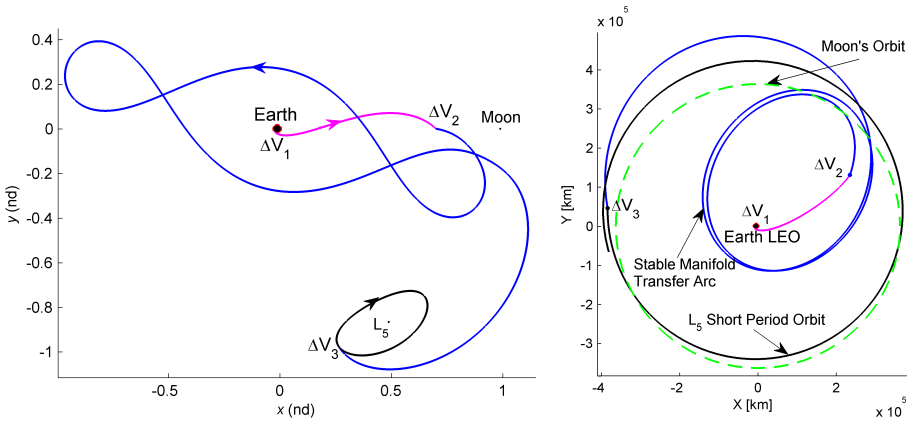

(a) Transfer A in Rotating Frame (b) Transfer A in Inertial Frame

Figure 11. Planar Transfer Trajectory A from Earth to an L_5 Short Period Libration Point Orbit

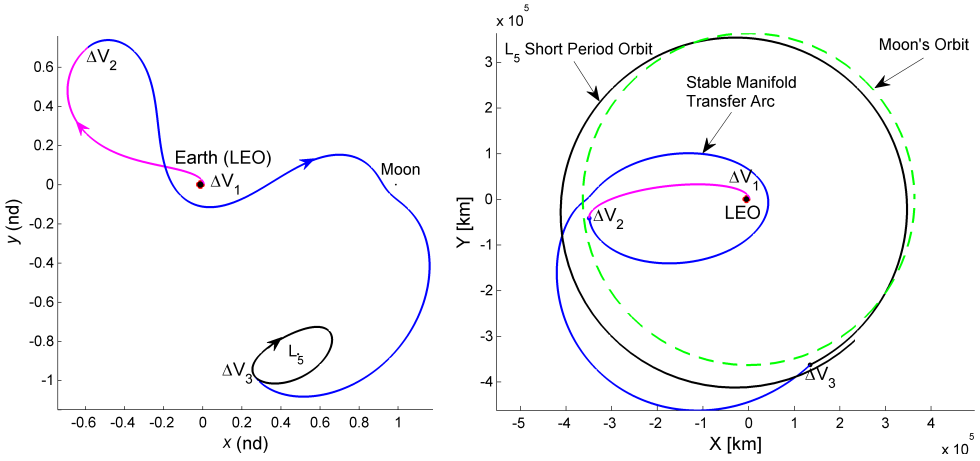

(a) Transfer B in Rotating Frame (b) Transfer B in Inertial Frame

Figure 12. Planar Transfer Trajectory B from Earth to an L_5 Short Period Libration Point Orbit

Figure 10. Transfer trajectory B, however, is the result of a slight modification of transfer A, that is, transfer trajectory A is used as an initial guess to construct a more direct transfer to the vicinity of L_5. To reduce the time of flight along the stable manifold arc, the location of the second maneuver ($\Delta\bar{V}_2$) is shifted from $y = 0$ to the second apoapsis along the stable manifold trajectory. At this location, a new tangential departure location along the circular Earth orbit is targeted in reverse time to yield a new Earth departure orbit. The energy level on this new departure leg is not constrained to equal the energy of stable manifold trajectory. As illustrated in Table 4, transfer B benefits from a reduction in time of flight as well as in total cost. Although there appears to be no significant change in direction at the three insertion locations, the total transfer cost along trajectory B is not reduced significantly. The magnitude of ($\Delta\bar{V}_2$) is reduced but the magnitude of ($\Delta\bar{V}_3$) is increased. Yet, the reduction in total time of flight is approximately 40% and the total maneuver cost is still decreased by 0.93%. The change in both direction and energy level as well as the reduction of flight time between the intermediate arcs is more apparent in the inertial frame. Thus, both transfers to

the vicinity of L_5 appear plotted in the inertial frame in Figure 11(b) and Figure 12(b). Note that the cost and time of flight associated with these transfers is not optimized. Rather the goal is a quick and efficient use of the maps to generate candidate transfers. Both transfers offer good initial guesses to seed different optimization schemes.

Three-Dimensional Transfer Trajectory from Earth

Strategies that exploit resonant orbits and manifolds to generate planar transfers are also applicable in the computation of three-dimensional transfers from Earth to out-of-plane periodic orbits in resonance with the Moon. To demonstrate the applicability of the invariant manifolds associated with 3D resonant orbits in the Earth-Moon system, an out-of-plane transfer from an inclined Earth parking orbit at 180 km altitude to a 3D periodic orbit of interest is detailed. The target three-dimensional periodic orbit is generated from a bifurcation in the planar family of orbits illustrated in Figure 1(h). The initial 3D periodic orbit emerging from the 2D bifurcating orbit is continued in z-amplitude. The effect of the Moon on the orbital period of these orbits in the 3D family is significant. Although the first member in this family possesses a near exact resonant period, that is, the period of the orbit is a near multiple of the orbital period of the Moon, as the family grows the period is reduced. Consequently, a spacecraft placed in one of the periodic orbits with a larger out-of-plane amplitude also possesses a closer approach to the Moon; the spacecraft completes three revolutions around the Earth in less time than that required for the Moon to complete two revolutions (54.5692 days). As the orbits in the family continue to increase in size, the orbital periods continue to decrease, and are, ultimately, 15 days shorter than the time interval in which the Moon completes two revolutions around the Earth. Nevertheless, these 3D periodic orbits are potentially useful for mission scenarios where a larger $\pm z$-amplitude is required but x- and y-amplitudes still remain between the Earth and the Moon. For instance, the selected out-of-plane orbit tours the entire system periodically - it passes through the vicinity of the collinear libration points L_1, L_2 and L_3 as well as the lunar south pole. Consequently, a vehicle placed in such orbit spends approximately 12 days below the orbital plane of the Moon. The period of the selected unstable orbit is 39.2545 days and the associated Jacobi constant value is $C = 2.9192$. For visualization purposes, different views of the 3D orbit appear in Figure 13. Note that the maximum z-component along this orbit is 60,424.9 km and the minimum z-component is -108,400.8 km.

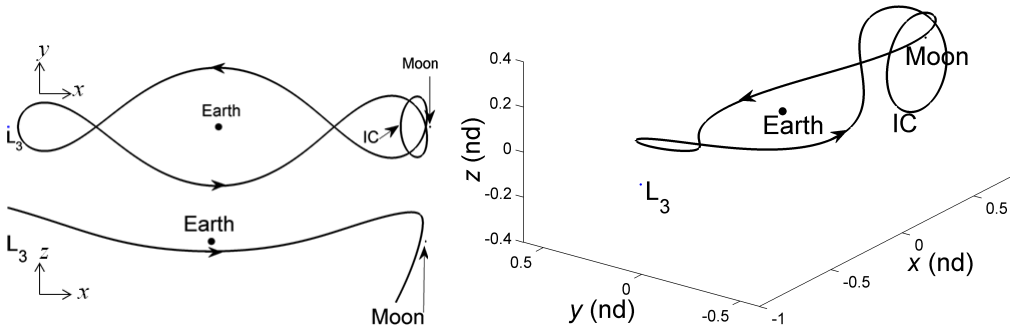

(a) xy- and xz-views (b) xyz-view

Figure 13. Three-Dimensional Periodic Orbit Selected from Out-Of-Plane Family of 3:2 Resonant Orbits Plotted in Figure 1(h) - Plotted in the Rotating Frame

A direct transfer trajectory from a low Earth orbit to the 3D periodic orbit in Figure 13 can be

costly due to the large out-of plane component. However, the instability of the orbit can be exploited and the invariant manifolds examined to search for stable manifold trajectories that travel to the vicinity of the Earth and possess a smaller z-component at Earth closest approach. A process similar to that used for planar transfers allows a search for potential low-cost connections between Earth departure trajectories and stable manifolds that asymptotically approach the 3D periodic orbit. First, the stable manifolds associated with the periodic orbit are computed and visualized in a projection of the surface of section at $y = 0$. A range of Earth departure trajectories is generated and plotted on the same map as illustrated in Figure 14. The stable manifolds again appear in blue and the various Earth departure trajectories are plotted in magenta.

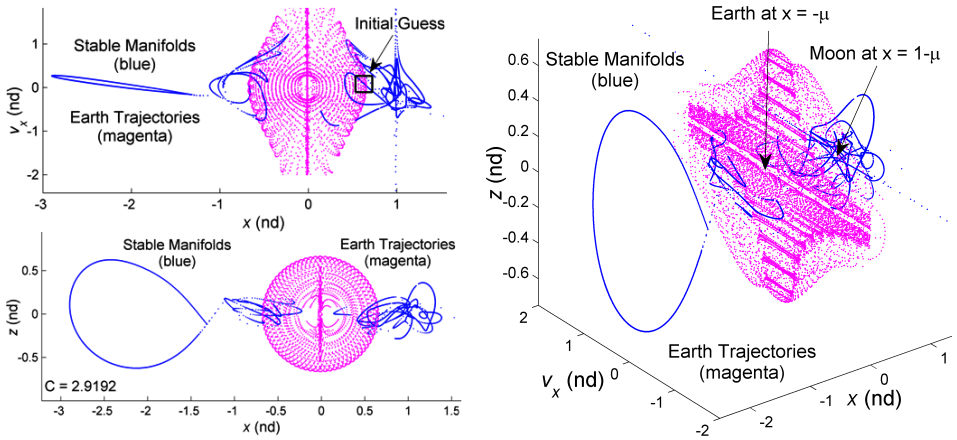

(a) xy-view (b) xz-view

Figure 14. Three-Dimensional Projection of the Surface of Section Illustrating the Stable Manifolds Associated with the Periodic Orbit in Figure 13 and the Earth Departure Trajectories

For the selected integration time interval (86 days) to reach the target orbit, it appears that there are no 'natural', maneuver-free connections between the stable manifolds and the Earth trajectories. If integrated for longer intervals, other connections may emerge but the time of flight also increases. Moreover, the manifold trajectories associated with resonant orbits, integrated for longer periods of time, become tangled and difficult to visualize even on the map. Thus, a nearby intersection is located on the map with arcs integrated for up to 86 days and the associated Earth departure and stable manifold arcs are integrated. The arcs then seed a corrections algorithm to correct the discontinuity that exists in position, allowing a maneuver at the connecting location to correct for the difference in velocity. To further reduce the initial maneuver ($\Delta\bar{V}_1$), the inclination of the initial departure orbit is allowed to vary. The stable manifold asymptotically approaches the target 3D orbit, thus, there is no requirement for a third maneuver to insert into the arrival orbit. The resulting transfer path is illustrated in Figure 15. The Earth departure arc is represented in magenta, the stable manifold arc appears in blue and the arrival 3D period orbit is plotted in black. The total cost ($\Delta\bar{V}_T$) and time of flight (TOF) associated with this transfer trajectory are detailed in Table 5. The time of flight along the Earth departure arc and along the stable manifold arcs are labeled TOF_E and TOF_M, respectively. For visualization purposes, the transfer trajectory is plotted in the inertial frame in Figures 15(d)-15(c); the out-of-plane component is more apparent in the xz-view. Note the excursion in the z-amplitude along the transfer path, crossing the Earth-Moon plane from above and below.

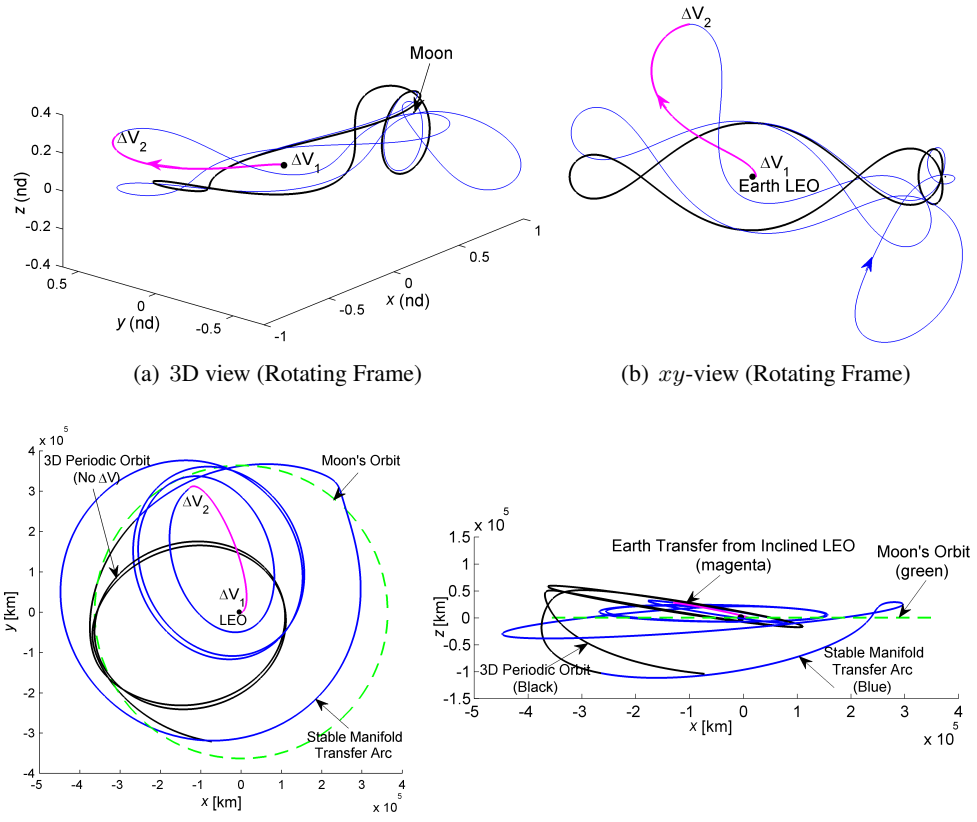

(a) 3D view (Rotating Frame)

(b) xy-view (Rotating Frame)

(c) xy-view (Inertial Frame)

(d) xy-view (Inertial Frame)

Figure 15. Three-Dimensional Transfer from an Earth Inclined Orbit ($i = 8.63$ deg) to the 3D Periodic Orbit in Figure 13 - Plotted in the Rotating Frame in (a)-(b) and in the Inertial Frame in (c)-(d).

Table 5. Maneuver Cost and Time of Flight Associated with 3D Transfer Trajectory

ΔV_1 (km/s)	ΔV_2 (m/s)	ΔV_T (km/s)	TOF_E (days)	$TOF_M(days)$	TOF (days)
3.1098	309.6728	3.4194	4.4735	64.7029	69.1764

A single selected 3D transfer scenario is detailed in this section to illustrate the possibility of accessing 3D periodic orbits from an Earth parking orbit for a reasonable cost and time of flight, but other scenarios are certainly available for this and other types of periodic orbits at various energy levels. Note also that the total cost and time of flight associated with this 3D transfer are sub-optimal. In fact, $\Delta\bar{V}_1$ and $\Delta\bar{V}_2$ can be optimized and a third potentially small maneuver could be inserted along the stable manifold arc to reduce the time of flight.

SUMMARY OF RESULTS AND CONCLUSIONS

A selection of interior and exterior planar and three-dimensional families of stable and unstable resonant orbits in the Earth-Moon system are computed. The gravitational influence of the Moon on these orbits reveals a variety of 3D resonant families and 3D transfer design scenarios. Poincaré sections are particularly effective in identifying two- and three-dimensional unstable resonant or-

bits and displaying the associated manifold structures. The design of 2D and 3D transfer trajectories is successfully applied in the Earth-Moon system. Planar and three-dimensional homoclinic- and heteroclinic-type trajectories are also generated with the aid of Poincaré maps. In particular, homoclinic- and heteroclinic-type connections are constructed for the planar and out-of-plane 1:2 and 2:3 resonant orbits.

As an application of the invariant manifold trajectories associated with unstable resonant orbits to preliminary mission design in the Earth-Moon system, two transfer trajectories are constructed and summarized. The problem of accessing the vicinity of L_5 from a 180-km low Earth orbit is examined by exploiting the stable manifolds associated with a planar 4:3 resonance. In addition, an out-of-plane transfer trajectory from a 180-km inclined low Earth orbit to a 3D periodic orbit that tours the entire Earth-Moon space is detailed.

ACKNOWLEDGMENT

The authors wish to thank the School of Aeronautics and Astronautics at Purdue University for supporting this work and the authors appreciate access to the computational facilities in the Barbara and Rune Eliasen Visualization Laboratory.

REFERENCES

[1] J. S. Parker and M. W. Lo, "Unstable Resonant Orbits near Earth and Their Applications in Planetary Missions," *AIAA/AAS Astrodynamics Specialist Conference*, Providence, Rhode Island, August 2004. AIAA 2004-22819.

[2] R. L. Anderson, "Low Thrust Trajectory Design for Resonant Flybys and Captures Using Invariant Manifolds," Ph.D. Dissertation, School of Aeronautics and Astronautics, University of Colorado, Boulder, Colorado, 2005.

[3] M. W. Lo, R. L. Anderson, G. Whiffen, and L. Romans, "The Role of Invariant Manifolds in Low Thrust Trajectory Design (Part I)," *AAS/AIAA Spaceflight Dynamics Conference*, Maui, Hawaii, February 2004. Paper AAS 04-288.

[4] R. L. Anderson and M. W. Lo, "The Role of Invariant Manifolds in Low Thrust Trajectory Design (Part II)," *AAS/AIAA Spaceflight Dynamics Conference*, Providence, Rhode Island, August 2004. Paper AIAA 2004-5305.

[5] M. W. Lo, R. L. Anderson, T. Lam, and G. Whiffen, "The Role of Invariant Manifolds in Low Thrust Trajectory Design (Part III)," *AAS/AIAA Spaceflight Dynamics Conference*, Tampa, Florida, January 2006. Paper AAS 06-190.

[6] M. Vaquero and K. C. Howell, "Poincaré Maps and Resonant Orbits in the Circular Restricted Three-Body Problem," *AAS/AIAA Astrodynamics Specialist Conference*, Girdwood, Alaska, July 31 - August 4 2011. Paper AAS-11-428.

[7] M. Vaquero, "Poincaré Sections and Resonant Orbits in the Restricted Three-Body Problem," M.S. Thesis, School of Aeronautics and Astronautics, Purdue University, West Lafayette, Indiana, 2010.

[8] C. D. Murray and S. F. Dermott, *Solar System Dynamics*. Cambridge, United Kingdom: Cambridge University Press, Cambridge, 1999.

[9] Carrico et al., "Lunar-Resonant Trajectory Design for the Interstellar Boundary Explorer (IBEX) Extended Mission," *AAS/AIAA Astrodynamics Specialist Conference*, Girdwood, Alaska, July 31 - August 4 2011. Paper AAS-11-454.

[10] McComas et al., "A New Class of Long-Term Stable Lunar Resonance Orbits: Space Weather Applications and the Interstellar Boundary Explorer," *Space Weather*, Vol. 9, November 2011, p. 9.

[11] R. L. Anderson and M. W. Lo, "Flyby Design Using Heteroclinic and Homoclinic Connections of Unstable Resonant Orbits," *21st AAS/AIAA Space Flight Mechanics Meeting*, New Orleans, Louisiana, February 13-17 2011. Paper AAS-11-125.